Published in final edited form as:
Proc Symp Haptic Interface Virtual Env Teleoperator Syst. 2011 July 11; 2011: 53–58. doi:10.1109/WHC.2011.5945461.

Optimizing Populations of SAI Tactile Mechanoreceptors to Enable Activities of Daily Living

Isabelle I. Rivest and **Gregory J. Gerling**
Department of Systems and Information Engineering, University of Virginia, Charlottesville, VA 22904

Isabelle I. Rivest: iir2u@virginia.edu; Gregory J. Gerling: gg7h@virginia.edu

Abstract

At present, the dense network of peripheral afferents between finger and brain and the large size of engineered sensors preclude the recreation of biologically observed afferent populations. This work uses a validated computational model of cutaneous skin and tactile afferents to evaluate sparse populations in performing tasks required in activities of daily living. Using a model (3D finite element representation of fingertip skin, linear bi-phasic transduction function, and leaky-integrate-and-fire neuronal model), we systematically varied populations of tactile receptors in dimensions of density (100, 45, 20, and 10 sensors/cm^2) and size (diameter 0.1, 0.2, 0.5, and 1.0 mm) to determine if a given modeled population can discriminate spheres and cylinders representative of objects used in activities of daily living. Using a scoring system which allows for direct comparisons between the populations, our results indicate that a population must have at least 20 sensors per cm^2 to maintain response resolution in these activities of daily living and that larger-sized sensors do not degrade response resolution.

Keywords

Tactile; touch; mechanoreceptor; solid mechanics; biomechanics; finite element analysis; leaky-integrate-and-fire; neural dynamics; neural prosthetics; psychophysics

1 Introduction

Replicating the dense population of mechanoreceptors in fingertip skin may augment current neural prosthetics [1]. However, present interfaces have at most 128 connections between device and cortex, mostly used for efferent control [2]. This leaves little spare connectivity for afferent feedback. Feedback to peripheral nerves is another option, though connecting artificial sensors to nerves on the order of 100/cm^2 is daunting and renders it nearly impossible to mimic receptor populations at densities observed in the finger. Additionally, current artificial sensors are larger than mechanoreceptors, and therefore dense populations cannot be mimicked without overlapping the sensors. While preliminary steps have been taken towards developing devices with integrated sensors [3], there remains a need for sparse arrangements of artificial sensors that maintain the resolution required to perform fundamental tasks.

Several scales have been developed that assess a person's ability to perform fundamental tasks required to care for themselves and live independently. These activities of daily living (ADL) include feeding, bathing, dressing, transfer/physical ambulation, and grooming. The execution of such activities is typically evaluated qualitatively in the clinic using Likert scales to rate patients [4].

Modeling techniques allow for the evaluation of reduced sensor populations. Previous efforts have sought to model mechanoreceptor behavior at the single-unit level and in populations. Skin models, for example, attempt to link the elasticity of the skin upon the indentation of spatial objects with the rate of elicitation of action potentials. Such models utilize continuum mechanics [5], [6] or finite element analysis (FEA) [7], [8]. In contrast, models that incorporate neural dynamics have sought to approximate the firing of individual action potentials. For example, the leaky integrate-and-fire (LIF) model has been used to predict the elicitation of action potentials in response to vibratory sinusoids and arbitrary noise stimuli [9], [10], [11]. Other empirical (non physics-based) models use regression techniques to relate spatial input to firing rate output. For example, Wheat and Goodwin modeled a single slowly adapting type I (SAI) afferent as a function of the curvature of annular stimuli and the distance between the stimulus and the mechanoreceptor's receptive field center [12]. However, since regression functions are associated with specific stimuli, they abstract underlying physiological mechanisms and must be re-fit to be used with stimuli of other shapes, sizes, and frequencies.

Built up from models of single-units, the response of populations of tactile receptors has been approximated using reciprocal interpretation, which explores a receptor's responsiveness as a stimulus probes spatially about its receptive field and extends this behavior to all receptors in a population [13]. For example, Guclu and Bolanowski used reciprocal interpretation to extend K.O. Johnson's single-unit work with RAs [14] to create populations with various spatial organizations and densities [15]. They defined unique quantitative (e.g., number of active fibers, summated firing rate, average firing rate) and qualitative (e.g., visual inspection of firing rates in spatial plot) dependent measures to investigate responses from several populations. In addition, Wheat and Goodwin have extrapolated their single-unit models to determine the effects of a population's density on neural resolution [12]. In addition to work with annular stimuli, they re-fit functions for curvature stimuli [16] and have considered impacts of a population's innervation geometry, noise, and non-uniform fiber sensitivity [17].

In order to determine how to reduce the tactile sensors in a population, the present work identifies specific tasks required to complete essential activities of daily living and from them abstracts representative objects, which serve as input into a validated, physics-based model of cutaneous skin and tactile afferents [18]. Population characteristics including sensor density, layout, and size are varied to investigate the inherent tradeoffs between these variables and response resolution.

2 Methodology

The objective of this work is to determine the effect of reduced sensor densities, various population layouts, and larger sensors on a population's ability to discriminate stimuli representative of objects used when performing activities of daily living. Three population-based, biological independent variables (population density, the geometric layout of sensors, and sensor size) are varied to determine their impact on overall response. A given combination of these variables is termed a 'population'. Additionally, two robustness independent variables (indenter location and indentation depth) were incorporated to judge a population's sensitivity to small perpendicular and lateral shifts of the indenter, as the experimental positioning of an indenter will vary by a small amount. A population's ability to discriminate two indenters was determined using a quantitative difference measure (summated Euclidian distance) and each population was scored on an ordinal scale based on the performance for several indenter pairs. Two discrimination tasks were considered (differentiating spheres and cylinders of varying radii).

2.1 Psychophysical Discrimination Tasks

The simulated tasks involve distinguishing spherical (Task 1) or cylindrical (Task 2) objects of various sizes. Indenters were constructed to represent idealized objects used in activities of daily living (transfer/physical ambulation, feeding, dressing, grooming, bathing, and responsibility for own medication). Eight indenters were created; four for each task. Spherical indenters with diameter 8, 20, 50, and 70 mm represent a variety of everyday objects such as medication, buttons, cabinet knobs, door knobs, baseballs, tennis balls, oranges, and joysticks on motorized wheelchairs. Cylindrical indenters of the same size correspond to pencils, spoons, toothbrushes, door handles, hand rails, and soda cans. Discriminating spheres with diameters 20 and 50 mm could correspond to differentiating a cabinet knob from a door knob using only the sense of touch. Figure 1 shows two examples of this mapping between real-world objects and idealized indenters.

2.2 Model

The model of the SAI mechanoreceptor (previously published [18]) transforms a static indentation of an arbitrary object into sequences of action potentials for each receptor in a population. From this sequence, firing rate is calculated over two time intervals; the dynamic ramp phase (30 – 50 ms) which is characterized by high spike firing during stimulus movement, and the static hold phase (650 – 900 ms) which is characterized by slower more regular firing during sustained indentation. Firing rate for a single receptor is validated by comparing model predictions to neural data recorded in experiments with primates [19]. Note that the receptive field size for a single-unit in the model is approximately 4 mm diameter. This is the area of the skin surface that when mechanically stimulated in the model leads to a non-zero value of strain energy density, as sampled at the position of the mechanoreceptors (1 mm deep). The receptive field size (as in the biology) differs from the volume of a Merkel cell – neurite complex (the end organ of the SAI) which is approximated by single elements in the model of 100 micron edge length. The population model is then validated by comparing firing rates of multiple receptors to the results of a psychophysical test of discrimination when the model is sampled at 100 sensors/cm^2, the density of SAIs in the human finger.

2.3 Numerical Experiments for Discrimination Tasks

The numerical experiments compare model output for a given population when indented with two stimuli of varying shapes to determine if they are distinguishable. Spheres with diameter 20, 50, and 70 mm are compared to the standard, a sphere with diameter 8 mm. Likewise, the three larger cylinders are compared to the smallest cylinder. These comparisons are made for each population and variability is taken into account through the use of two robustness variables.

2.3.1 Independent Variables—Three biological variables and two robustness variables were changed in performing the numerical experiments. Population density, geometrical layout, and sensor size (Figure 3) relate directly to the population configuration and were varied to determine their effect on discrimination ability. Four densities (100, 45, 20, and 10 sensors/cm^2), three geometrical layouts (rectangular, random, and Gaussian random) and four sensor sizes (0.1, 0.2, 0.5, and 1.0 mm diameter) were considered for a total of 48 populations. Additionally, each stimulus was indented to three depths (0.75, 1.00, and 1.25 mm) and in three locations on the fingertip (0.00, 0.25, 0.50 mm shift). The indenter was shifted towards the base of the finger along the proximal-distal axis.

2.3.2 Dependent Variable—A quantitative dependent metric, per sensor Euclidian distance, is defined and calculated for each indenter comparison. Populations are then scored on an ordinal scale based on the per sensor Euclidian distance measurements.

Per sensor Euclidian distance: Per sensor Euclidian distance (Eqn 1, 2) measures the similarity between two indenters as indicated by the firing rates elicited over a given population. The distance between the firing rate elicited by one sensor when indented with the standard stimulus and that elicited by the same sensor when indented with the comparison stimulus is summed over all sensors in the population. This value is calculated for all sensors in a given population and summed, then divided by the number of active sensors, sensors with non-zero firing rates when indented with either the standard or comparison indenter. Thus, the per sensor Euclidian distance measures the difference between firing rates when one population is indented with multiple indenters.

$$\bar{d}_d = \frac{1}{a_d} \sum_{i=0}^{n} \sqrt{\left[(dyn\_f_{std})_i - \left(dyn\_f_{comp}\right)_i \right]^2} \quad (1)$$

$$\bar{d}_s = \frac{1}{a_s} \sum_{i=0}^{n} \sqrt{\left[(stat\_f_{std})_i - \left(stat\_f_{comp}\right)_i \right]^2} \quad (2)$$

In equation 1, $\bar{d}_d$ is per sensor Euclidian distance in the dynamic ramp phase, a_d is the number of active sensors in this phase, n represents the total number of sensors, and $(dyn\_f_{std})_i$ and $(dyn\_f_{comp})_I$ are the dynamic firing rates elicited by sensor i when indented with the standard and comparison indenters, respectively. Eqn. 2 is the same calculation for the static phase.

Per sensor Euclidian distance was calculated for each stimulus comparison over all combinations of the robustness variable for a total of 36 data points (4 comparisons × 3 depths × 3 shifts) for each population arrangement and for both the dynamic ramp and static hold phases.

Figure 2 is a hypothetical plot showing per sensor Euclidian distance for a population exhibiting the desired behavior. The subscript for per sensor Euclidian distance is dropped on this plot, indicating that the same process was followed for both phases. Three features make the combination of biological variables in Figure 2 a strong population for differentiating sets of indenters. First, the magnitude for per sensor Euclidian distance for each comparison is large. This indicates a large difference in model behavior when stimulated with objects of different sizes. Second, per sensor Euclidian distance is smallest when comparing the standard indenter to the indenter with diameter 20 mm and largest when comparing the standard to the indenter with diameter 70 mm. This corresponds to a firing rate behavior that indicates not only that the indenters being compared are dissimilar, but also that the smaller indenters are more similar to the standard than larger indenter. Lastly, the error is small for all four comparisons, indicating that the population configuration is robust to indenter depth and location. These three features, termed the order, variance, and magnitude conditions (detailed further below) make up the basis of a system for scoring populations.

Population scoring: Response in the dynamic ramp and static hold phases was scored for each of the 16 combinations of biological variables. A score of 0 to 3 points was given for each of the magnitude, order, and variance conditions for a total of 9 points for either indenter shape. Scores for the spherical and cylindrical indentations were then summed for a

maximum of 18 points per population. The scoring procedure presented below is detailed elsewhere [14].

Magnitude condition: Three, one sample t-tests were performed to determine whether each of the comparisons of dissimilar indenters within a population was significantly larger than 0 at α=0.01, where μ_i represented the true mean per sensor Euclidian distance when comparing the standard to stimulus with diameter i, where i={20, 50, 70}. A population received 0 points if each comparison could not be rejected in favor of the alternative hypotheses (i.e. not significantly larger). If the three null hypotheses were rejected at α=0.01, a population received 1 to 3 points based on the magnitudes of $\bar{x}_{20}$, $\bar{x}_{50}$, $\bar{x}_{70}$, the sample averages for the comparison of the standard to the stimulus with diameter 20, 50, and 70, respectively. A population received 3 points if $\bar{x}_{20}$, $\bar{x}_{50}$, $\bar{x}_{70}$ were each in the 75th percentile when compared to the distribution of averages within one comparison indenter over all populations. A population received a 2 if all of $\bar{x}_{20}$, $\bar{x}_{50}$, $\bar{x}_{70}$ were in the top 50th percentile, and a 1 otherwise.

Order condition: Three, two-sample t-tests were performed to determine whether the standard and comparison stimuli yielded significantly different per sensor Euclidian distance at α=0.25. This condition ensures that the model can correctly identify that the comparison indenter with diameter 20 mm is more similar to the standard than the comparison indenter with diameter 50 mm. A population received 3 points if the comparisons of dissimilar indenters were rejected in favor of the alternative hypotheses, 2 points if any two null hypotheses were rejected, 1 point if one null hypothesis was rejected and 0 points if the null hypothesis could not be rejected for any of the tests.

Variance condition: The standard deviation for each comparison in a population was binned according to its standing over all populations. A population received 3 points if all 4 comparisons yielded a standard deviation in the bottom 30%. Two points were awarded if 2 comparisons yielded a standard deviation in the bottom 30% and the third was not in the top 10%. One point was awarded if 1 comparison yielded a standard deviation in the bottom 30% and the remaining two were not in the top 10%. Zero points were awarded for populations with standard deviations in the top 10% or with no standard deviations in the bottom 30%.

3 Results

This section presents population response results for the discrimination tasks in the numerical experiments. Figure 4 shows per sensor Euclidian distance ($\bar{d}$) as a function of comparison indenter diameter for one combination of sensor layout, population density, and sensor size. The blue plot lines represent the response in the dynamic ramp-up phase and green plot lines correspond to the static hold phase. Note that results presented in this section are highly dependent on the chosen discriminability measure, per sensor Euclidian distance. While this measure does not have a direct biological correlate, it quantifies the difference in firing rates elicited by a given population when stimulated with various indenters.

As stated above, the ideal population has three characteristics: 1) large magnitude, 2) monotonically increasing, and 3) little variability. While many populations exhibit these features, some populations (not all are shown here) do not conform to these requirements. A drastic drop in magnitude occurs between populations with sensor density 20 sensors/cm^2 and 10 sensors/cm^2 for almost all of the populations considered. This is an indicator that a sensor density of 10/cm^2 is inadequate for the discrimination of objects in the selected tasks.

To analyze the results quantitatively, population characteristics were mapped onto an ordinal scale according to the three desirable traits. Populations are scored from 0 to 9 for each of the 2 tasks, totalling a possible 18 points. Scoring results for the dynamic ramp and static hold phases are shown in Table 1. The validated population, a rectangular population with sensor density 100 sensors/cm^2 and sensor size 0.1 mm, achieves scores of 10 and 9 for the dynamic ramp and static hold phases, respectively. Thus, a score of 10 or better indicates a strong population, 7-10 indicates a reasonably strong population, and a score of 6 or below denotes a poor population.

Figure 5 shows that population rating increases as sensor density increases. Figure 7, which plots population rating as a function of sensor size, does not show any increasing or decreasing trends, but the range and variance of population scores increase as sensor size increase. Figure 7 displays sensor density, sensor size, and population score in 3 dimensions. Since sparse densities and large sensors are ideal, the best populations are the data points residing in the top back quadrant.

4 Discussion

The work develops a scoring system for comparing responses from populations of peripheral afferents. By mimicking two psychophysical discrimination tasks involving activities of daily living, populations with various densities, sensor layouts, and sensor sizes are evaluated to determine which configurations are best suited for these tasks. The scoring system allows the rating of sensor configurations based on their performance in three categories: magnitude, order, and variance. This allows for direct comparisons between populations. We note, however, that the discriminatory mechanisms of the somatosensory cortex are presently unknown. Therefore, while our scoring system provides a quantitative means of estimating how to reduce the number of artificial sensors, it does not accurately capture, and likely oversimplifies, how the central nervous system functions.

Overall, dense populations consistently score the highest, while the sparsest populations score poorly. This evidence suggests the tool has strong predictive validity. The ability of a population to discriminate spheres and cylinders of different sizes is consistently strong for populations with sensor densities of 100 sensors/cm^2. Likewise, populations with 10 sensors/cm^2 are not effective when performing these tasks in almost every case. Results for populations of density 45 and 20 sensors/cm^2, however, have more nuanced results and require specific combinations of the biological independent variables. A final recommendation for prosthetic designers is to employ 45 sensors/cm^2 with a Gaussian sensor layout and large (1.0 mm) sensors. Note 45 sensors/cm^2 corresponds to approximately 11 sensors in a 0.5 mm × 0.5 mm area. However, this recommendation changes to a rectangular population with 0.5 mm sensors for designers utilizing sensor densities of 20 sensors/cm^2. Additionally, results indicate that cylinders of different size are more difficult to discriminate than spheres. Therefore, we need to select populations based on a specific task. Finally, populations with smaller sensors did not consistently score better than identical populations with larger sensors. This is beneficial due to constraints on manufactured sensors. Future work could investigate sensors larger than 0.1 mm. Additionally, we do not consider noise present in neural responses, within and between afferents, though this could be added to the model.

References

1. Chapin JK, Moxon KA, Markowitz RS, Nicolelis MAL. Real-time control of a robot arm using simultaneously recorded neurons in the motor cortex. Nature Neuroscience. Jul.1999 2:664–670.

2. Hochberg LR, Serruya MD, Friehs GM, Mukand JA, Saleh M, Caplan AH, Branner A, Chen D, Penn RD, Donoghue JP. Neuronal ensemble control of prosthetic devices by a human with tetraplegia. Nature. Jul.2006 442:164–171. [PubMed: 16838014]

3. Dhillon GS, Horch KW. Direct neural sensory feedback and control of a prosthetic arm. IEEE Transactions on Neural Systems and Rehabilitation Engineering. Dec.2005 13:468–472. [PubMed: 16425828]

4. Katz S, Ford AB, Moskowitz RW, Jackson BA, Jaffe MW. Studies of Illness in the Aged; The Index of ADL: A Standardized Measure for Biological and Psychosocial Function. Journal of the American Medical Association. Sep.1963 185:914–919. [PubMed: 14044222]

5. Johnson KO, Phillips JR. Tactile Spatial Resolution. I. Two-Point Discrimination, Gap Detection, Grating Resolution, and Letter Recognition. Journal of Neurophysiology. 1981; 46:1177. [PubMed: 7320742]

6. Sripati AP, Bensmaia SJ, Johnson KO. A continuum mechanical model of mechanoreceptive afferent responses to indented spatial patterns. Journal of Neurophysiology. Jun.2006 95:3852–3864. [PubMed: 16481453]

7. Dandekar K, Raju BI, Srinivasan MA. 3-D finite-element models of human and monkey fingertips to investigate the mechanics of tactile sense. Journal of Biomechanical Engineering-Transactions of the ASME. Oct.2003 125:682–691.

8. Srinivasan MA, Dandekar K. An investigation of the mechanics of tactile sense using two-dimensional models of the primate fingertip. Journal of Biomechanical Engineering-Transactions of the ASME. Feb.1996 118:48–55.

9. Freeman AW, Johnson KO. A Model Accounting for Effects of Vibratory Amplitude on Responses of Cutaneous Mechanoreceptors in Macaque Monkey. Journal of Physiology-London. 1982; 323:43–64.

10. Bensmaia S. A transduction model of the Meissner corpuscle. Mathematical Biosciences. Apr.2002 176:203–217. [PubMed: 11916509]

11. Looft F. Response of Monkey Glabrous Skin Mechanoreceptors to Random Noise Sequences: II. Dynamic Stimulus State Analysis. Somatosensory and Motor Research. 1996; 13:11–28. [PubMed: 8725645]

12. Wheat H, Goodwin A. Tactile discrimination of edge shape: limits on spatial resolution imposed by parameters of the peripheral neural population. Journal of Neuroscience. 2001; 21:7751–7763. [PubMed: 11567065]

13. Mountcastle VB, Powell TP. Neural mechanisms subserving cutaneous sensibility, with special reference to the role of afferent inhibition in sensory perception and discrimination. Bull Johns Hopkins Hosp. Oct.1959 105:201–32. [PubMed: 14424738]

14. Johnson KO. Reconstruction of population response to a vibratory stimulus in quickly adapting mechanoreceptive afferent fiber population innervating glabrous skin of the monkey. Journal of Neurophysiology. 1974; 37:48–72. [PubMed: 4204567]

15. Guclu B, Bolanowski SJ. Modeling population responses of rapidly-adapting mechanoreceptive fibers. Journal of Computational Neuroscience. Apr.2002 12:201–218. [PubMed: 12142551]

16. Goodwin AW, Browning AS, Wheat HE. Representation of curved surfaces in responses of mechanoreceptive afferent fibers innervating the monkey's fingerpad. Journal of Neuroscience. Jan.1995 15:798–810. [PubMed: 7823181]

17. Goodwin AW, Wheat HE. Effects of nonuniform fiber sensitivity, innervation geometry, and noise on information relayed by a population of slowly adapting type I primary afferents from the fingerpad. The Journal of Neuroscience. 1999; 19:8057–8070. [PubMed: 10479706]

18. Rivest, I.; Gerling, GJ. Proceedings of the 2010 IEEE Haptic Interfaces for Virtual Environment and Teleoperator Systems. Boston, MA: 2010. Evaluating populations of tactile sensors for curvature discrimination; p. 59-62.

19. Phillips JR, Johnson KO. Tactile Spatial Resolution. II. Neural Representation of Bars, Edges, and Gratings in Monkey Primary Afferents. Journal of Neurophysiology. 1981; 46:1192–1203. [PubMed: 6275041]

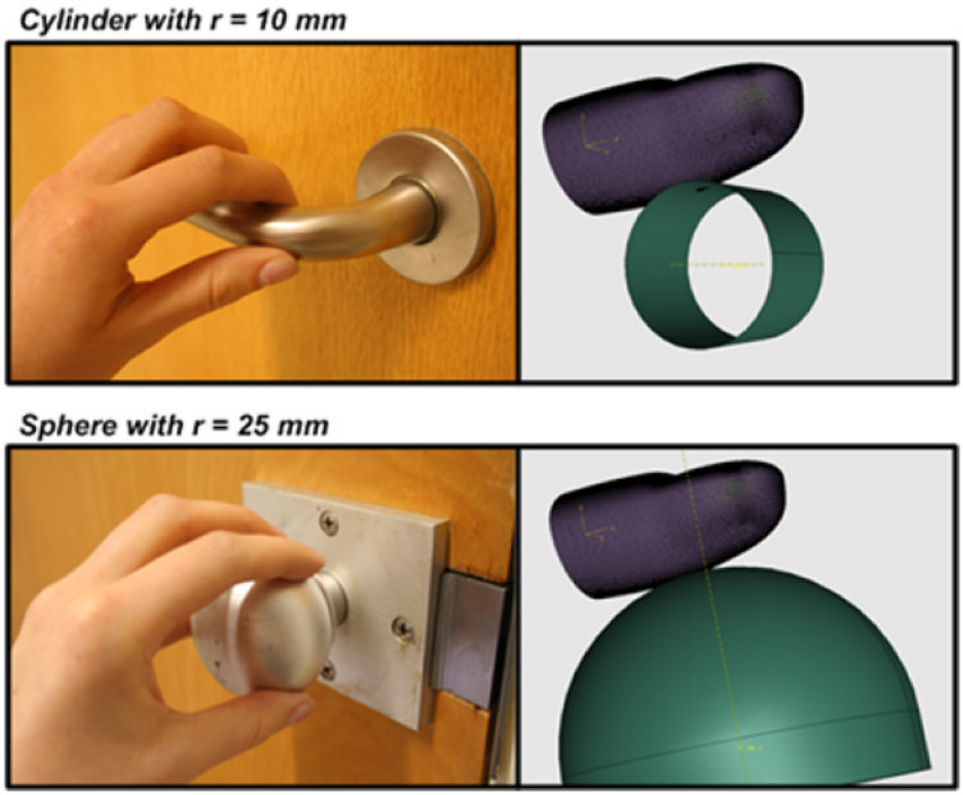

Figure 1.
Mapping real-world objects to idealized primitives.

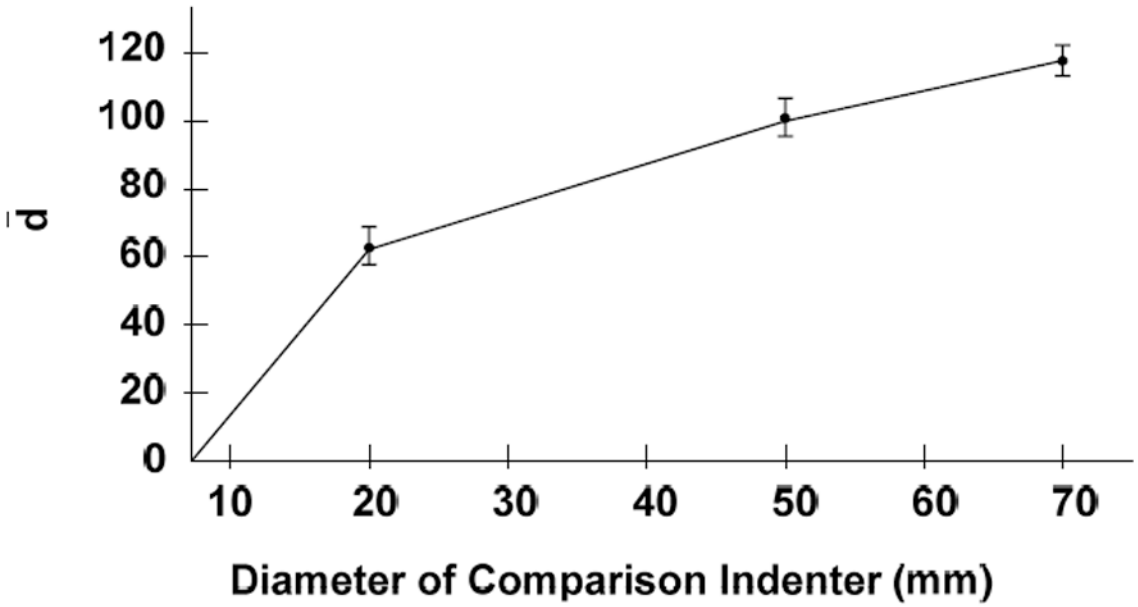

Figure 2.
Idealized comparison plot showing per sensor summated Euclidian distance for three comparison indenters with a standard of diameter 8 mm.

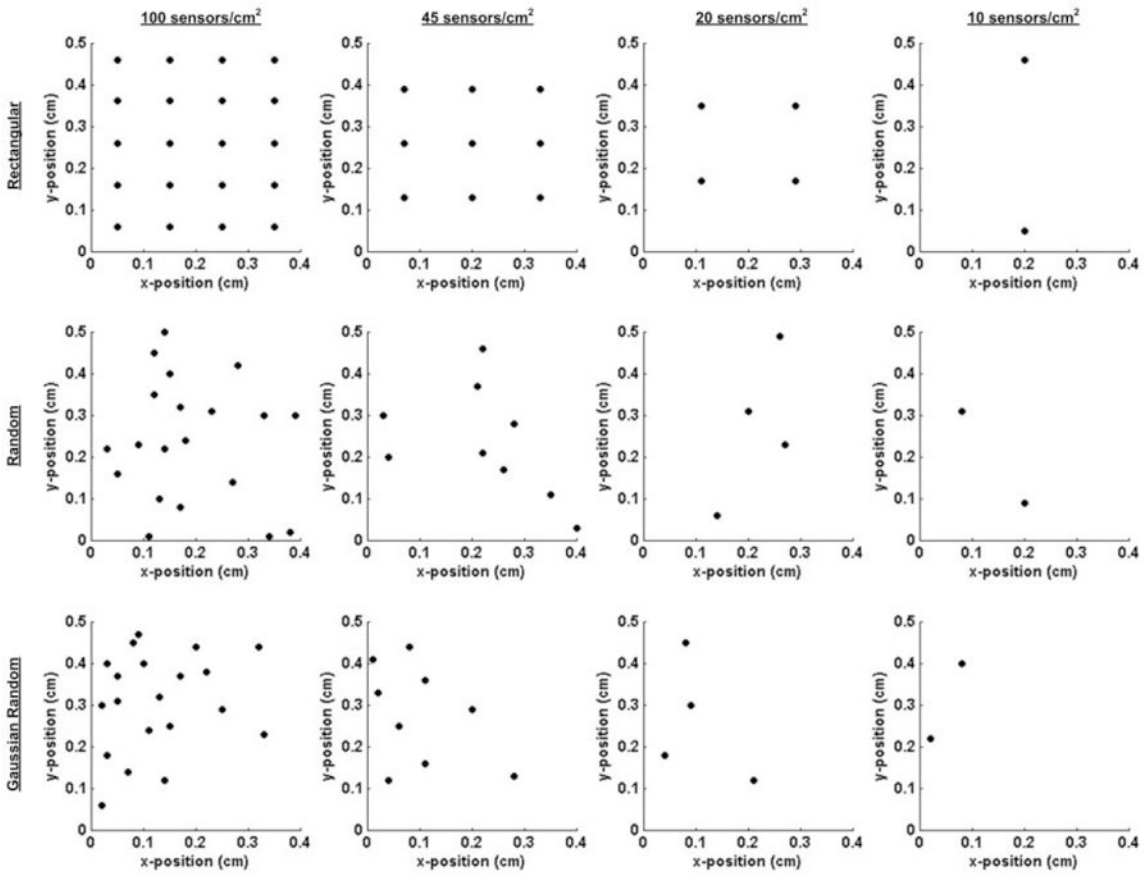

Figure 3.
Sensor distribution for two biological variables: population layout and density. The area used was a 4.0 × 5.0 mm rectangle

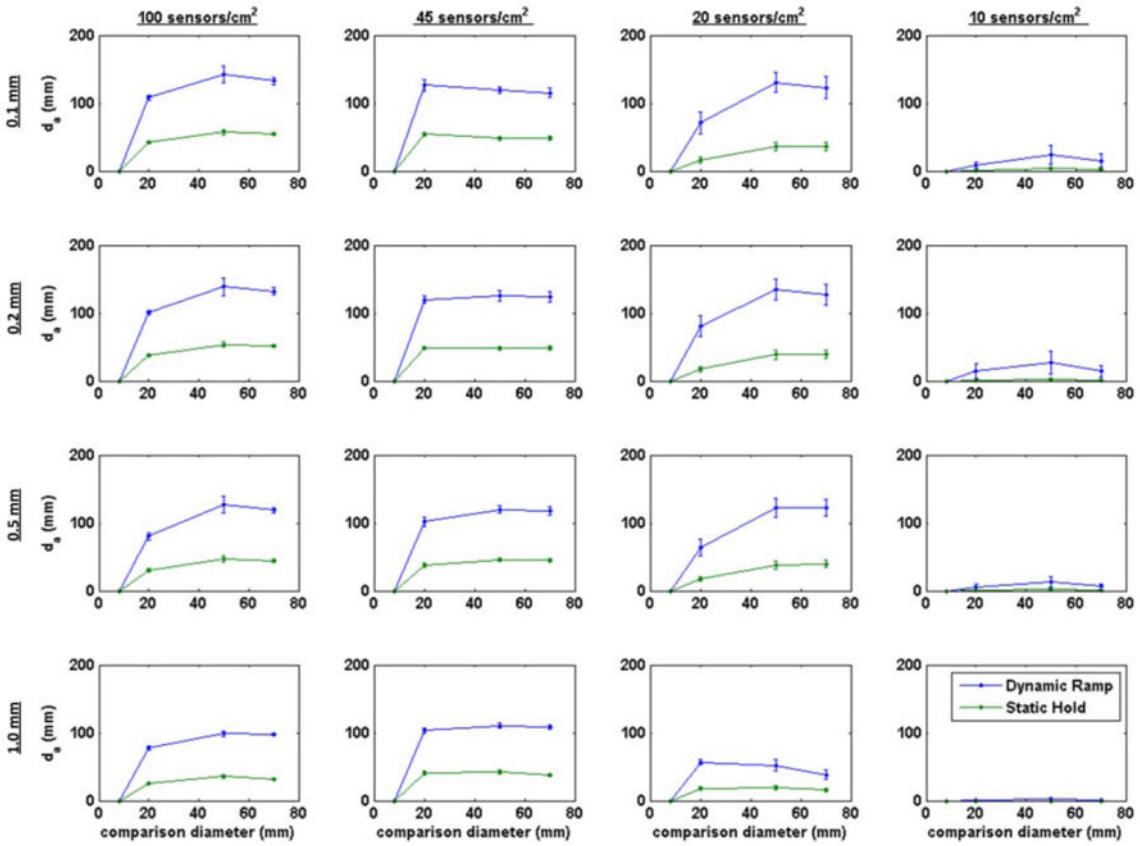

Figure 4.
Results for the random population layout when indented with spherical stimuli.

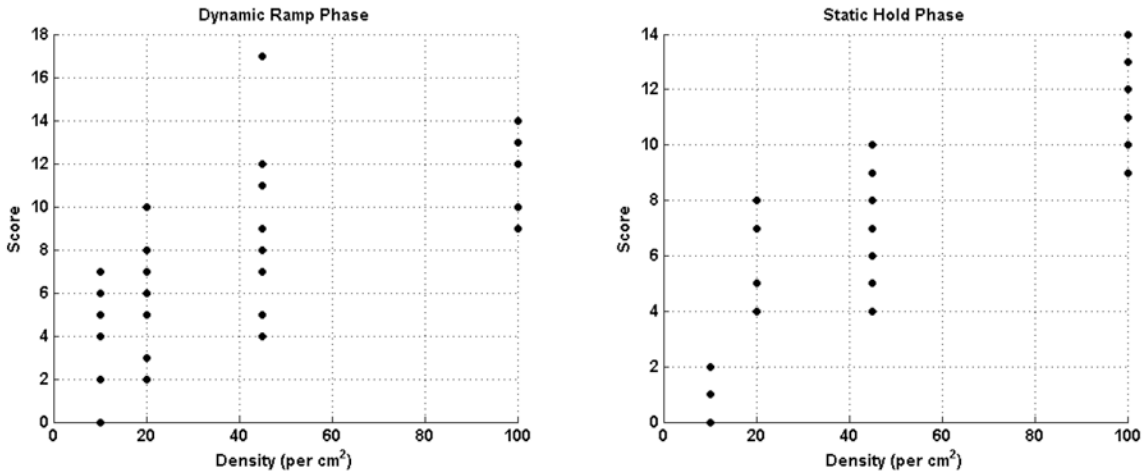

Figure 5.
Population score as a function of sensor density.

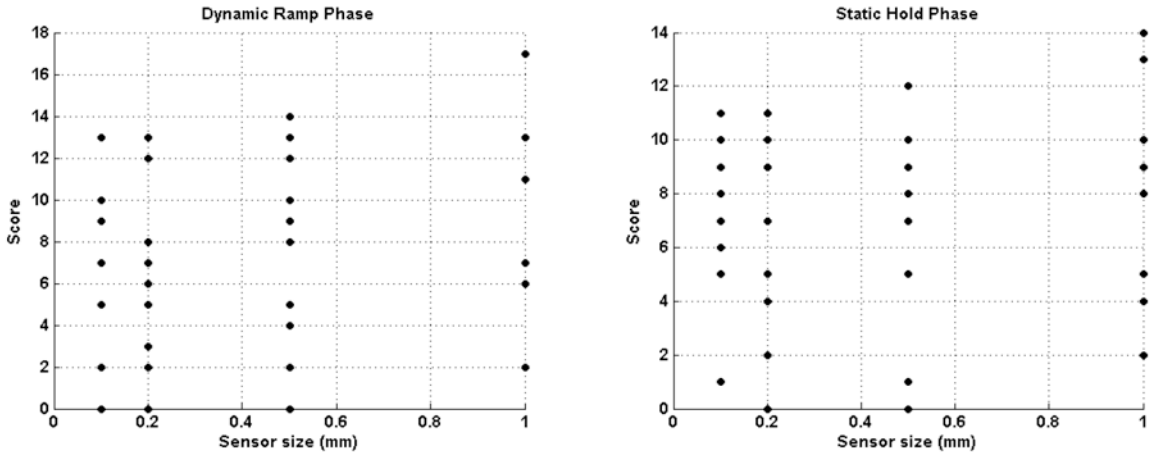

Figure 6.
Population score as a function of sensor size.

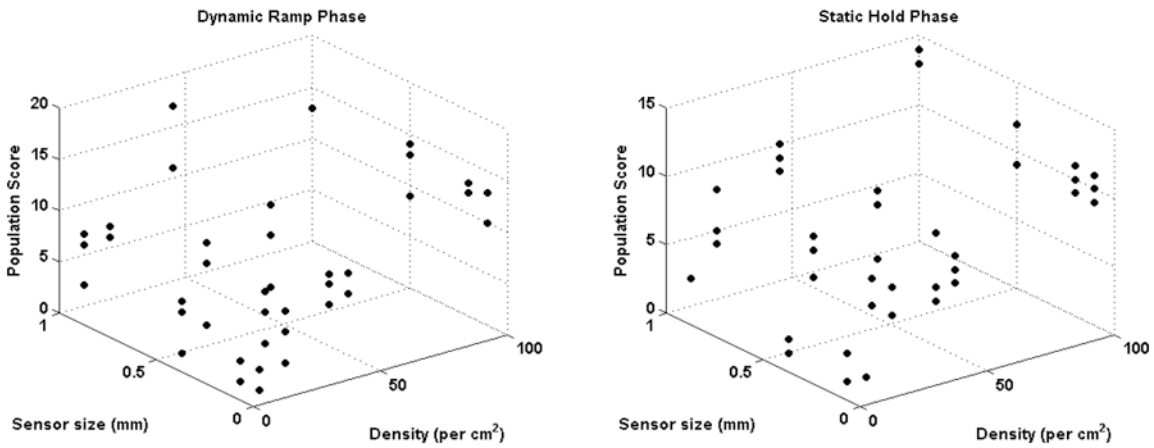

Figure 7.
Population score as a function of sensor density and sensor size.

Table 1

Rating results, where higher scores tie to populations that better discriminate spheres and cylinders of varying size.

	Dynamic Ramp	Static Hold	Dynamic Ramp	Static Hold	Dynamic Ramp	Static Hold	Dynamic Ramp	Static Hold	
0.1 mm	10	9	9	6	7	7	2	1	*Rectangular*
	13	11	7	8	5	7	2	1	*Random*
	13	10	9	7	2	5	0	1	*Gaussian*
0.2 mm	12	10	5	4	6	7	2	2	*Rectangular*
	13	9	7	5	8	7	0	0	*Random*
	12	11	8	9	3	5	0	0	*Gaussian*
0.5 mm	9	9	4	5	10	8	0	0	*Rectangular*
	14	12	9	9	8	7	4	1	*Random*
	13	12	12	10	2	5	5	1	*Gaussian*
1.0 mm	13	13	11	10	7	4	2	2	*Rectangular*
	13	14	11	9	7	5	6	2	*Random*
	13	13	17	9	6	8	7	2	*Gaussian*
	100/cm^2		**45/cm^2**		**20/cm^2**		**10/cm^2**		

Proc Symp Haptic Interface Virtual Env Teleoperator Syst. Author manuscript; available in PMC 2012 May 11.